

Design and expected performance of an MCAO system for the Giant Magellan Telescope

N. Mark Milton, Michael Lloyd-Hart, Andrew Cheng,
James A. Georges III, and J. Roger Angel

Center for Astronomical Adaptive Optics, The University of Arizona, Tucson, AZ 85721

ABSTRACT

Adaptive optics will play a crucial role in achieving the full potential of the next generation of large diameter telescopes. In this paper, we present an optical design for a multi-conjugate adaptive optics system for the Giant Magellan Telescope, a 25.7 m telescope with a primary mirror consisting of seven 8.4 m segments. The tri-conjugate MCAO optics is based on adaptive secondary technology developed for the MMT telescope and incorporates dynamic refocus optics for the laser guide star wavefront sensors. We use the results of analytic (non-Monte-Carlo) numerical simulations to determine the optimal configuration of deformable mirrors as well as laser and natural guide stars. The simulation results are extended to include and quantify the effects of wavefront sensor and control loop delay noise as well as dynamic refocus and fitting error on the expected system performance and sky coverage.

Keywords: adaptive optics, multi-conjugate adaptive optics, numerical simulation, extremely large telescopes

1. INTRODUCTION

The Giant Magellan Telescope (GMT)¹ is a concept being explored by the Magellan partners to create a Giant Segmented Mirror Telescope (GSMT) from 25.7 m telescope units. In the 20/20 configuration,² two telescope units move on a 100 m track to provide coherent interferometric imaging with four times the resolution of a single 30 m telescope with the same total area. Each GMT unit telescope will have a fast, compact structure with a primary mirror ($f/0.7$) consisting of seven 8.4 m mirror segments. The key design parameters for a GMT unit telescope are summarized in Table 1.

Table 1. GMT unit telescope design parameters

Effective aperture	21.7 m
Edge-to-edge aperture	25.7 m
Primary Mirror	$f/0.7$, 18 m fl
Primary segments	seven 8.4 m (round)
Gregorian deformable secondary	3.7 m, $f/7.7$

Adaptive optics will be essential to the successful coherent interferometric beam combination from multiple GMT units as well as in achieving the full potential of the individual GMT unit telescopes when operated independently.

In this paper, we describe a multi-conjugate adaptive optics (MCAO) system design for an individual GMT unit telescope (shown in Figure 1). We present a tri-conjugate MCAO system consisting of three deformable mirrors (DM) based on the adaptive secondary mirror (ASM) technology which is being used at the MMT telescope. A combination of natural guide stars (NGS) as well as sodium (SLGS) and Rayleigh (RLGS) laser guide stars are used to sense the optical aberration induced by atmospheric turbulence. Dynamic refocus³⁻⁶ optics collect laser light over a range of heights into a small spot to increase the number of photons available for wavefront sensing and to improve the accuracy of the turbulence measurements.

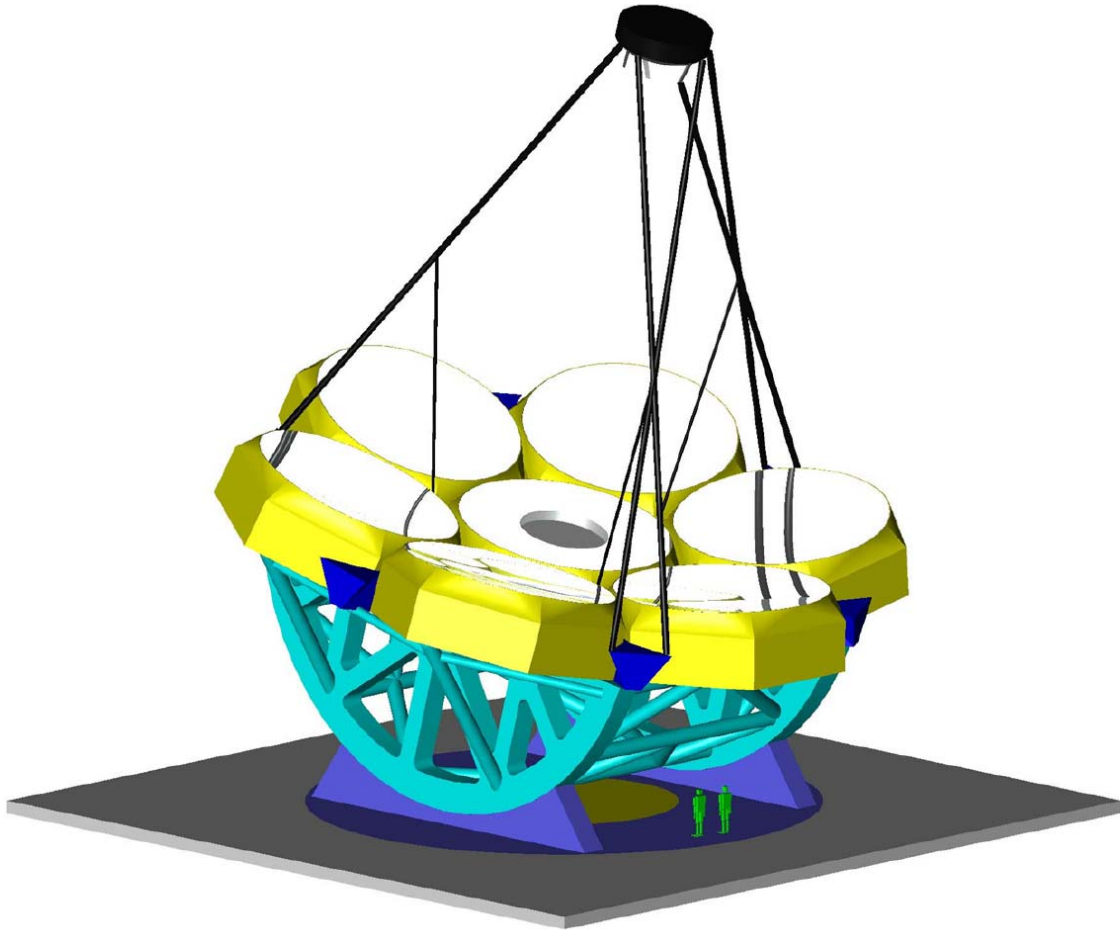


Fig. 1. GMT unit telescope with fast segmented primary, adaptive deformable secondary, and compact support structure (image courtesy S. Gunnels).

We use the results of analytic numerical simulations to determine the optimal conjugate heights for the deformable mirrors and to select the best configuration of laser and natural guide stars for wavefront sensing after considering a range of beacon geometries. The simulation results are extended to include and quantify the effects of wavefront sensor and control loop delay noise as well as dynamic refocus and fitting error on the expected system performance and sky coverage.

We show that a high level of correction can be achieved for science imaging in the infrared with a consistent PSF across a 2 arcmin field of view (FOV) using natural and laser guide stars selected from within a 2 arcmin and 2.6 arcmin FOV respectively. Rayleigh beacons are used, instead of multiple NGSs, to fully correct the vertical distribution of second order aberrations across the FOV.⁷ Rayleigh beacons also provide some additional information on low order aberrations to improve the isoplanatic correction near the edge of the field. Finally, Rayleigh beacons permit the use of a single NGS for sensing global tilt which in turn allows the GMT to achieve nearly full sky coverage.

The results of the simulations motivate a design for the GMT MCAO optical system for science imaging at the diffraction limit from $1.6 - 10\mu m$. We present a description of the deformable mirrors, relay optics, dynamic refocus optics, wavefront sensors (WFS), and science imaging system along with an analysis of the optical performance at both the science and WFS image planes.

2. NUMERICAL MODELING

2.1. Description of the code

Numerical simulations have been carried out to explore the performance of a range of GMT MCAO beacon geometries and DM conjugate heights and to determine the GMT MCAO performance under expected noise conditions. The MCAO model for these simulations has been developed in the C++ programming language and supports an arbitrary number of LGS, NGS, DMs, and atmospheric turbulence layers. The model assumes the geometric optics approximation. Noise due to limited photon flux, sky background, and read noise is computed assuming a Shack-Hartmann WFS is used for each laser and natural guide star.

Atmospheric aberration and DM corrections are represented by vectors of coefficients for Zernike modes. An analytic computation is used to obtain the modal influence of aberration at each layer (\mathbf{I}_L) and DM (\mathbf{I}_{DM}) within the intersecting cone for each LGS and NGS. The resulting Zernike coefficient vectors make up the columns of these influence matrices. The model simulates the effects of dynamic refocus for RLGS and SLGS by averaging the wavefronts over the range of beacon heights weighted by the laser return flux from each height.

A maximum a posteriori reconstructor matrix^{8,9} \mathbf{R}_{DM} is computed from the DM influence matrix through

$$\mathbf{R}_{DM} = \left(\mathbf{I}_{DM}^T \mathbf{C}_n^{-1} \mathbf{I}_{DM} + \mathbf{C}_a^{-1} \right)^{-1} \mathbf{I}_{DM}^T \mathbf{C}_n^{-1} \quad (1)$$

where \mathbf{C}_a is the open-loop atmospheric modal covariance matrix¹⁰ computed at the respective DM heights, and \mathbf{C}_n is the beacon modal noise covariance matrix. The tomographic reconstructor matrix used in this simulation is computed by taking the product of the DM reconstructor and the atmospheric layer influence matrix

$$\mathbf{T} = \mathbf{R}_{DM} \mathbf{I}_L \quad (2)$$

and gives the DM modal prescription directly from a given set of atmospheric layer turbulence modes.

The noise free residual compensated wave-front error \mathbf{E} for an object at infinity is computed⁷ as a function of field angle for each Zernike aberration mode applied to each atmospheric layer. The mean square residual phase error contributed by each mode in the stellar wave front is then given by⁹

$$\epsilon = \text{diag}(\mathbf{E} \mathbf{C}_a \mathbf{E}^T) . \quad (3)$$

The total error summed over all modes for all layers is then just given by $\sigma_T^2 = \text{Tr}(\mathbf{E} \mathbf{C}_a \mathbf{E}^T)$.

The analytic simulation performance is dramatically faster than simulations which rely on point-by-point computation of phase maps. In addition, the analytic manipulation of modal coefficients also provides increased accuracy by avoiding discrete sampling errors.

2.2. Modeled system

The model simulates the performance of a GMT unit telescope with seven 8.4 m primary mirror segments with a full aperture width of 25.7 m. The central mirror segment has a 3 m hole to accommodate instruments at the Cassegrain focus. The Gregorian ASM also has seven segments mirroring the geometry of the primary mirror, and is conjugated 150 m above the ground. Two additional DMs are conjugated at 6 km and 12 km. Each DM corrects Zernike modes through order 30 over a compensated field of view of 60 arcsec radius. The ground-layer DM is allowed to correct all modes, while the 6 km and 12 km conjugate DMs are restricted to Zernike orders two and above and three and above respectively.

Details of the 7-layer model atmosphere are shown in Table 2, which give a turbulence-weighted mean height \bar{h} of 5090 m and r_0 of 0.15 m at a wavelength of 0.5 μm . This profile reflects preliminary SCIDAR measurements made above Mt. Graham and Mt. Hopkins in Arizona¹¹ supplemented by simultaneous weather balloon measurements of wind speed and direction. In this simulation, the ground layer turbulence is located at 200 m above the secondary mirror conjugate height.

Table 2. Model atmosphere

Height (m)	r_0 (m) at 0.5 μm	Fraction of total power	Wind Speed (m/s)	Wind Direction (deg)
200	0.29	0.34	10.3	215
2000	0.78	0.07	5.1	250
3400	0.41	0.19	7.2	270
6000	0.63	0.09	16.5	269
7600	0.78	0.06	23.2	259
13300	0.39	0.21	22.7	259
16000	1.05	0.04	5.7	067

Five 10 W sodium beacons are modeled in a regular pentagon with 1.0 arcmin radius. We anticipate that a hologram will be used to create all five spots from a single 50 W laser, as shown recently for Rayleigh beacons by Georges et al.⁶ The laser is expected to generate pulses at 5 kHz with a duty cycle of just 2% to prevent interference between successive pulses. This can lead to high peak power, but we believe saturation effects in the sodium layer will not be significant; they have been ignored in this simulation. Each pulse is range gated and refocused from 90–100 km. The beam projector is modeled with $d/r_0 \approx 4$ mounted behind the secondary mirror to produce short exposure diffraction limited spots in the mesosphere of 0.60 arcsec.¹² The simulation assumes a spot size of 0.75 arcsec to allow for 0.005 arcsec beacon jitter¹³ and 0.45 arcsec of dynamic refocus error.⁵ Five 50×50 Shack-Hartmann WFSs sense Zernike modes in orders 2–30 from each SLGS beacon (15×15 spots across each 8.4 m aperture segment). Each SLGS WFS is assumed to have a platescale of 1.5 arcsec per pixel, 40% throughput, and read noise of $3 e^-$ RMS.

Five 5 W Rayleigh beacons are projected in a regular pentagon with 1.3 arcmin radius. The simulation assumes lasers at 351 nm, whereas we expect now to use frequency doubled YAG at 532 nm, but the difference in SNR is small. Each pulse is range gated and refocused from 25–27.5 km. Spot sizes of 0.75 arcsec are also assumed for the Rayleigh beacons. Five 6×6 Shack-Hartmann WFSs sense just second order Zernike modes from each RLGS spot (2×2 spots across each 8.4 m aperture segment). Other parameters for the WFSs are assumed to be the same as for the SLGS.

Finally, an additional WFS senses tilt modes only from a natural guide star in the J- and H-bands. In practice, the NGS will be selected from the science channel with a pick-off mirror and is expected to have a nearly diffraction limited spot size due to the correction provided by the MCAO system. The full 25.7 m aperture is used to measure tilt, and the sensor is assumed to be a single avalanche photo-diode (APD) quadcell with a platescale of 0.2 arcsec per pixel, 40% throughput, and zero read noise.

2.3. Optimization of DM conjugate heights and LGS configurations

The selection of optimum DM conjugate heights and a preliminary selection of optimal guide star geometries requires the evaluation of the performance of a very large number of MCAO system configurations. Each variation of DM height and guide star direction has a unique reconstructor matrix. Simulations were performed for the noise free case using the analytic calculation of the tomographic matrix \mathbf{T} and the total mean square residual phase error σ_T^2 for each MCAO configuration as a function of FOV. The criterion for selecting the optimal MCAO geometry was the lowest RMS error that remained approximately constant across the 2 arcmin FOV.

The conjugate height of the ASM was fixed at 150 m above the ground. Simulations were run in which the conjugate heights of the 2nd and 3rd DMs were allowed to range from 1 km to 16 km. As expected, the performance of the MCAO system was not very sensitive to selection of conjugate height.⁷ The MCAO performance with DM heights at 6 km and 12 km produced optimum results with performance varying by only a few tens of nanometers RMS as the DM heights varied by ± 1 km. This variation in performance was small compared to the effects of varying the guide star geometry. Therefore, DM heights of 6 km and 12 km were selected for the optical design.

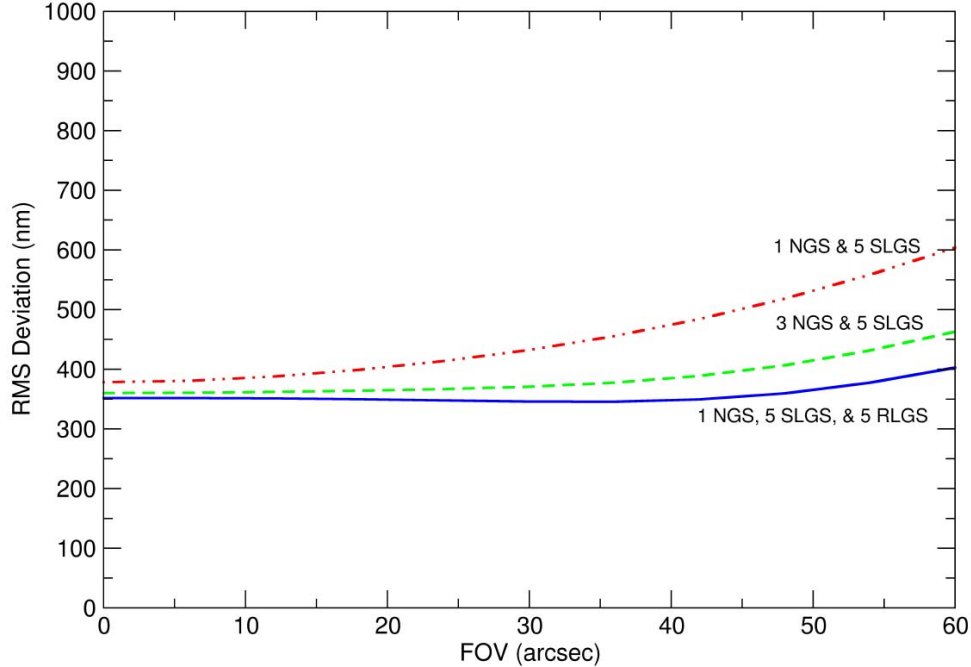


Fig. 2. GMT noise free performance including dynamic refocus and fitting error.

Performance was evaluated also for a range of guide star geometries. SLGS configurations including from one to three rings of beacons and between 4 and 7 beacons per ring were examined. The opening half-angle for the beacon rings ranged from 0.1 arcmin to 1.5 arcmin.

The results showed that two SLGS rings provided a small improvement over a single ring. The optimum SLGS ring radius for a single ring was 1 arcmin, and for a second ring was 1.3 arcmin. Further improvement was negligible when a third ring was added. Five beacons per ring produced improved performance over 4 beacons, with only a small additional improvement when 6 and 7 beacons were included in each ring.

The most significant change in MCAO performance resulted from the use of multiple natural guide stars or the inclusion of a single ring of Rayleigh laser beacons. The model includes, in the first case, 3 NGS sensing tip-tilt only, and in the second, a pentagon of RLGS sensing only second order modes. Both cases provide the necessary height diversity for a complete solution of the vertical distribution of second order aberrations,⁷ which cannot be done with additional SLGS. This allows the 3 DM MCAO system to fully correct first and second order modes across the whole 2 arcmin FOV, resulting in substantially less field dependence of the PSF.

Figure 2 illustrates this effect in a configuration that includes a single SLGS pentagon at 1 arcmin. The five RLGS are located at 1.3 arcmin. The 3 NGS are placed in an equilateral triangle at 0.4 arcmin although simulation results showed that performance degraded only slightly if they were placed at random, but non-colinear, locations within the 2 arcmin FOV.

Indeed, the Rayleigh beacons provide improved performance over a configuration with 3 NGS since they yield some additional information on low order aberrations to improve the isoplanatic correction near the edge of the field. The Rayleigh beacons have the further advantage of requiring the use of only a single NGS to sense global tilt, resulting in improved sky coverage.

The MCAO configurations using a single pentagon of SLGS along with either 3 NGS or a single NGS plus a pentagon of RLGS were selected for more detailed simulations under expected noise conditions.

2.4. System performance under expected noise conditions

Detailed simulations, including the effects of WFS and photon noise, control loop delay, as well as dynamic refocus and fitting error, were performed on the selected beacon geometries. A design goal for the MCAO system was to achieve full sky coverage in H band and longward. Table 3 lists the minimum visual magnitude range that provides the required 1 NGS and 3 NGS configurations within the modeled 2 arcmin FOV based on predicted differential star counts in the I-band¹⁴ for two selected fields at 30° galactic latitude and one field at the galactic pole. These simulations use NGS with magnitudes at the upper end of these ranges to be conservative.

Table 3. Expected NGS count within 2 arcmin FOV

Galactic Latitude (deg)	Avg. NGS in FOV	m_v
+30	1.1	16-17
	3.0	18-19
+90	1.2	18-19
	2.8	20-21

Atmospheric turbulence was simulated as sums of Zernike modes computed for each layer over the full metapupil. Simulated Zernike time series coefficients were computed for each atmospheric layer. The Zernike modal temporal power spectrum¹⁵ calculated for the atmospheric layer metapupil dimensions, coherence length r_0 , and wind speed and direction determines the amplitude of each temporal frequency for each Zernike mode. The Zernike time series coefficients were computed from an inverse Fourier transform with a random phase for each frequency. The model simulates the effects of servo lag as a pure delay in these time series of 2 ms; twice the WFS integration time of 1 ms.

For these early simulations, DM corrections were applied up to radial order 30, or 495 modes. For a telescope of the size of the GMT, fitting error is therefore the limiting residual aberration. Corrections are computed as the product of the the time series turbulence Zernike coefficient vectors and the tomographic reconstructor matrix. Shack-Hartmann WFS noise is calculated from WFS RMS tilt error¹⁶ due to photon and read noise propagated through a Shack-Hartmann WFS reconstructor matrix and the reconstructor matrix \mathbf{R}_{DM} .

The performance of each MCAO configuration is evaluated by calculating the average RMS deviation along 10 different lines of sight from the optical axis out to a field angle of 1 arcmin. The RMS deviation in each direction is averaged over 10 azimuthal angles for each of 100 widely spaced temporal samples of atmospheric turbulence. The fit error due to unsensed and uncorrected turbulence¹⁰ for Zernike modes of order $n > 30$ is added in quadrature to the RMS deviation.

Figure 3 illustrates this effect of noise on the selected MCAO configurations. The brightness of the single NGS used with the RLGS configuration was $m_v = 17.3$ which provides ≈ 1.1 NGS within the 2 arcmin FOV at 30° galactic latitude. For the 3 NGS configuration, the NGS brightness was $m_v = 19.3$ which provides ≈ 3.0 NGS within the 2 arcmin FOV at the same latitude. The overall performance of 3 NGS is reduced compared to the RLGS configuration because of the lower signal to noise ratio on the fainter stars.

At the galactic pole, simulations using a single NGS with $m_v = 19.3$, providing ≈ 1.2 NGS within the 2 arcmin FOV, and a RLGS ring still produce good performance with a consistent RMS error of 400 nm across the FOV. However, three NGS with a brightness of $m_v = 21.3$, providing only ≈ 2.8 NGS within the 2 arcmin FOV at the galactic pole, exhibit seriously degraded performance because of insufficient signal to noise ratio, due to a high H-band sky background level,¹⁷ on the NGS tilt measurements.

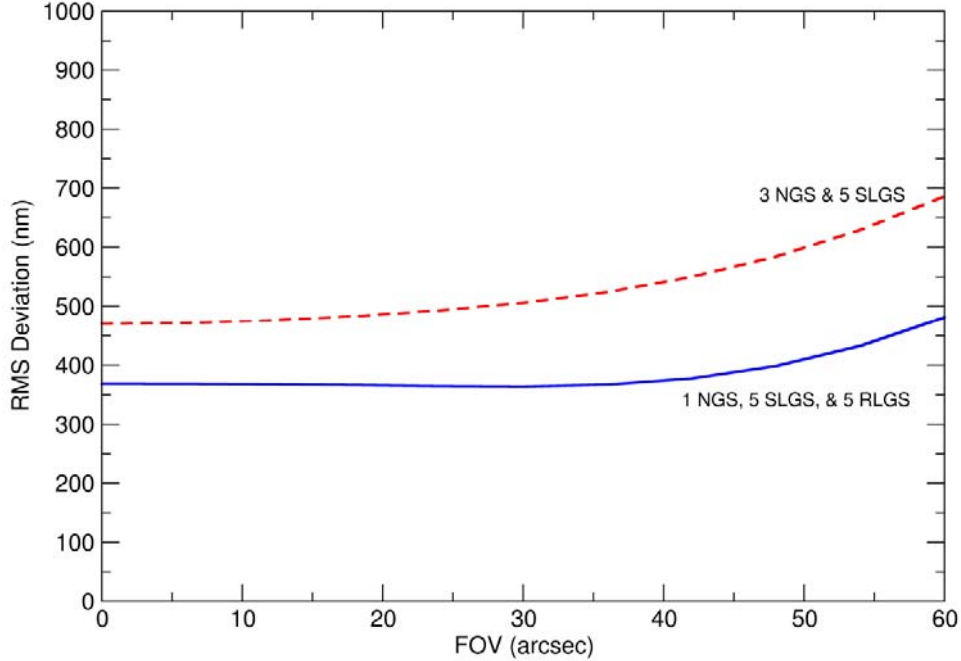


Fig. 3. GMT performance including dynamic refocus and fitting error as well as WFS and control loop time delay noise at 30° galactic latitude.

3. TRI-CONJUGATE ADAPTIVE OPTICS DESIGN

The overall layout of the telescope with the MCAO system mounted at the Cassegrain focus is shown in Figure 4. The Gregorian ASM has the same segmented geometry as the primary and brings the light to a focus at $f/7.7$ behind the primary mirror cell. The primary forms an image of the ASM at a height of 150 m above the ground, ideal for correction of ground layer turbulence. Beam projectors for the Rayleigh and sodium laser beacons, including the holograms to split the laser light five ways, will be located behind the secondary mirror.

Figure 5 shows the path of rays traveling from the Cassegrain focal plane. The 2^{nd} DM, which is a 0.82 m $f/1.5$ asphere, is conjugated to a height of 6 km and corrects for turbulence at intermediate altitudes. A folding flat in the shadow of the secondary mirror redirects the light to the 3^{rd} DM which is conjugated to a height of 12 km. This DM is a 0.48 m $f/1.75$ asphere.

After the DMs, light from astronomical sources is collimated, while LGS light will be slightly diverging. The resulting aberrations, largely spherical, are corrected in the succeeding WFS relay optics. Coming off the third DM, light from all sources enters the cryogenic dewar through a flat window, where two narrow-band notch reflectors in series separate the light from the Rayleigh beacons at 532 nm, and the sodium beacons at 589 nm. The Rayleigh channel is placed first to allow the possibility of long wave pass dichroic beam splitters instead. Separate exit ports on the dewar transmit the LGS light to the respective dynamic refocus units, while longer wavelengths continue into the dewar. The exit ports in fact are lenses that reduce the beam size for LGS light.

The Rayleigh and sodium dynamic refocus and WFS optics will be mounted in a fixed position on the back of the primary mirror cell. Neither they nor the DMs will be mounted to a field rotator, and so will remain fixed with respect to the telescope. This means that rotation of the LGS spot pattern on the sky will not be necessary, but in order to maintain a fixed geometry between the sky and the science focal plane, the optical elements below the perforated diagonal flat in the science channel will be mounted on a rotator within the dewar.

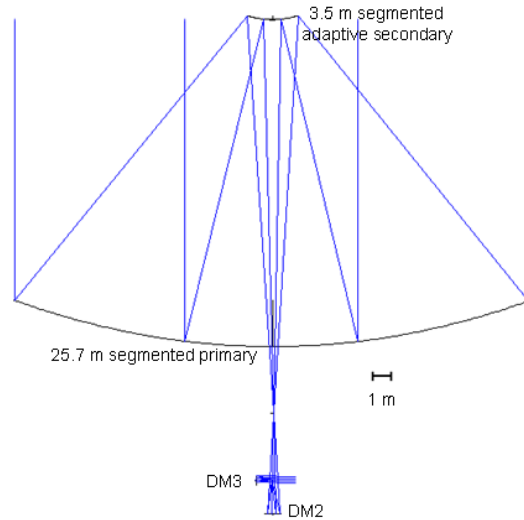


Fig. 4. GMT primary, ASM, and 2nd and 3rd DM optics.

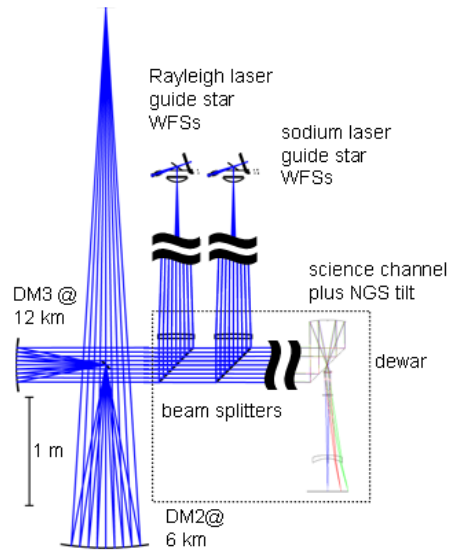


Fig. 5. GMT 2nd and 3rd DM optics, Rayleigh and sodium beacon relay optics, and science channel.

3.1. Wavefront sensing and dynamic refocus optics

Figure 6 illustrates the dynamic refocus and WFS reimaging optics for the Rayleigh beacons. The sodium beacon WFS channel is very similar, with optics of slightly different prescription, except that the fixed focus position is further back due to the beacons' higher altitude. In both cases, the field lens (bottom) relays the pupil to a point just in front of the dynamic refocus system. The flat mirror (top) is perforated so that incoming rays for each beacon are reflected into the dynamic refocus optics (left) but pass through the a hole diagonally opposite to the original beacon footprint into the WFS optics (right). The $f/0.5$ spherical movable mirror in each dynamic

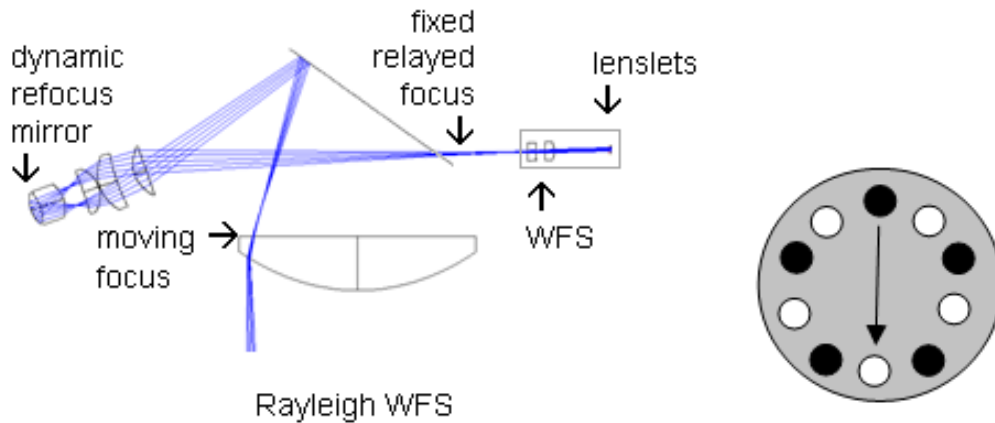


Fig. 6. (Left) Rayleigh beacon dynamic refocus and WFS optics. (Right) Perforated flat mirror with holes (white) for rays from corresponding WFS light footprints (black).

refocus assembly takes the moving focus point resulting from the range of beacon conjugate heights, located behind the field lens, to a fixed focus point in front of the WFS optics.

The required motion for the Rayleigh dynamic refocus mirror is $\pm 160 \mu\text{m}$ at 2.5 kHz, which subjects the mirror to an acceleration of 16,000 g. For the sodium channel, the requirement is a little milder: $\pm 100 \mu\text{m}$ at 5 kHz and acceleration of 10,000 g. For comparison, the Rayleigh beacon dynamic refocus already demonstrated at the 61" Kuiper Telescope on Mt. Bigelow has a mirror whose movement is $\pm 80 \mu\text{m}$ at 5 kHz and 8,000 g.⁶

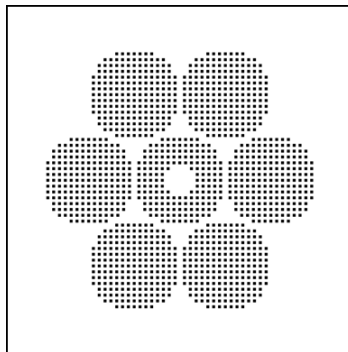


Fig. 7. WFS spot pattern formed on the sodium WFS CCDs by the segmented pupil. The dimensions of the 256×256 CCD are represented by the solid border.

The WFS reimaging lenses map the exit pupil of the refocus unit onto the lenslet arrays which are located 1.3 mm in front of the WFS CCDs. Figure 7 shows the Shack-Hartmann spot pattern produced on the sodium WFS CCDs with 15×15 spots per 8.4 m primary mirror segment. The $144 \mu\text{m}$ $f/20$ lenslet array chosen in this design is a close match to an existing AOA part and the 256×256 CCD ($20 \mu\text{m}$ per 0.2 arcsec at $f/20$) with a 1 kHz frame per second readout rate is similar to CCDs currently available from MIT/Lincoln Labs.

Figure 8 shows spot diagrams for the Rayleigh and sodium WFS channels at the fixed relayed focus just before the WFSs themselves. In both cases, the image size is much smaller than the expected image size in a single subaperture, which for the sodium channel may be as low as the diffraction limit of 0.22 arcsec, but for the Rayleigh, with its large subapertures, will be the seeing limit. The maximum slope error across any WFS subaperture is 0.076 arcsec for the sodium channel, and 0.035 arcsec for the Rayleigh channel.

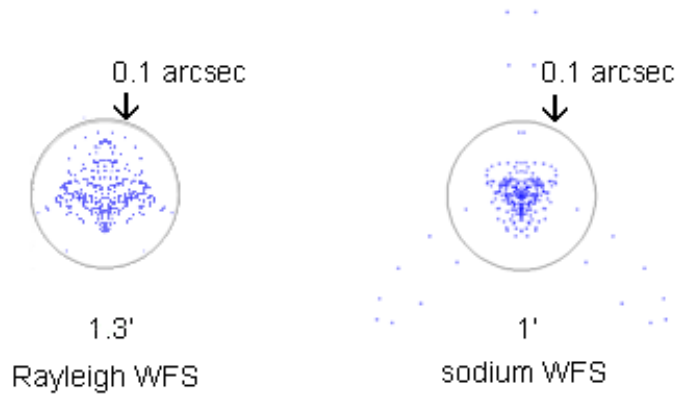


Fig. 8. (Left) Rayleigh beacon spot diagram. (Right) Sodium beacon spot diagram.

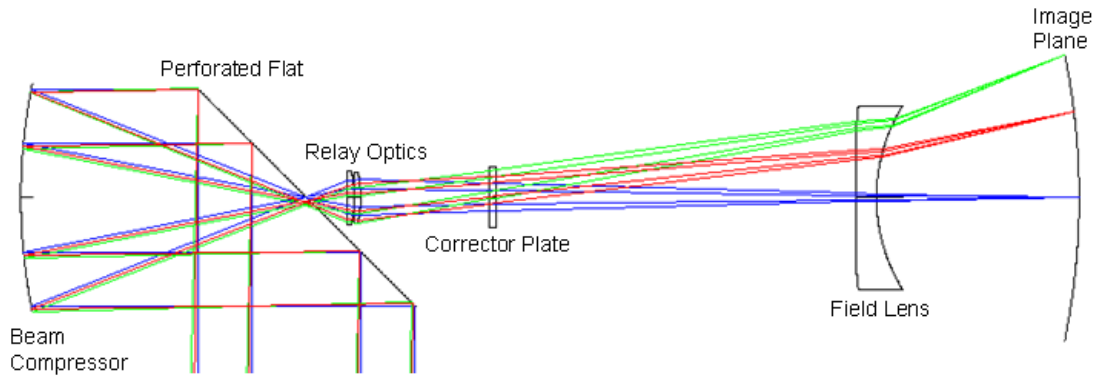


Fig. 9. GMT science channel optics.

3.2. Science imaging optics

Figure 9 illustrates the science channel reimaging optics. A pupil image is formed on the flat mirror, which has a central hole within the shadow of the secondary mirror. The flat sends light to a reflective beam compressor which serves to reduce the beam size, permitting the use of small, manufacturable, IR lenses. It also produces an accessible intermediate focal plane at the position where the rays pass through the central hole in the flat mirror. A pick-off mirror in this image plane will be used to select a natural guide star for tilt sensing within the science field.

ZnSe relay optics form a final exit pupil in front of the corrector plate. Baffling at this exit pupil will be used to control stray light. There are only two optical elements located beyond the exit pupil: a ZnSe corrector plate and a CaF₂ field lens.

Figure 10 shows the spot diagrams for the science focal plane which has a radius of curvature of 1 m. The enclosing circles represent the position of the first Airy minimum for the diffraction limited spots at 1.6 μm wavelength. These beams have wavefront errors of 0.002 μm RMS (on-axis), 0.011 μm RMS (0.6 arcmin), and 0.036 μm RMS (1 arcmin). The final focal ratio is $f/29$, allowing focal plane arrays with 18 μm pixels to provide Nyquist sampling in H-band.

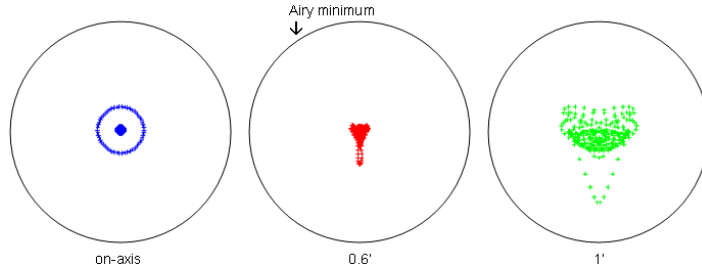


Fig. 10. Science image plane spot diagrams for on-axis, 0.6 arcmin and 1 arcmin radial positions in the field.

4. CONCLUSIONS

MCAO for telescopes in the 30 m class holds great promise for imaging with exquisite resolution over a wide field. We find however that even with a collecting area equivalent to a 22 m filled aperture, achieving all sky coverage limits us to a single NGS for tilt sensing in the sparsely populated regions of the Galactic pole. But with such limited information on low-order aberrations from beacons at different heights, PSF uniformity over the field is badly compromised.

Fortunately, Rayleigh laser beacons can be employed to provide extra information. Since only second order modes need be sensed, the beacons need not be bright and low power lasers gated over 2.5 km are sufficient. We find that excellent performance over the field is obtained with five 10 W SLGS, five 5 W RLGS, and a single NGS of $m_v < \sim 19$. On the timescale for production of the GMT, we can expect sodium lasers of 50 W to be available; 25 W doubled YAG lasers already are, and so the practical requirements on the beacons do not seem daunting.

Dynamic refocus of both types of LGS is required, but the optical design allows one mechanism to compensate focus for all 5 beacons of each type. For the RLGS in fact, given the small number of subapertures, the light for all the beacons can be put on a single CCD whose requirements can already be met by, for example, the E2V CCD39. The SLGS require a 256×256 device with very low noise and probably 32 readout amplifiers for each beacon. Even so, this is not a major advance in the current state of the art.

By using large curved aspheric DMs that build on demonstrated techniques developed for adaptive secondary mirrors, an optical design for the MCAO system of great efficiency is possible. Furthermore, stability of the optical servo loop can be assured with the explicit feedback of actuator positions provided by the DMs.

In addition to correction to the near-IR diffraction limit offered by the full-blown MCAO system, the first stage, that is, the adaptive secondary mirror, can be used on its own as a corrector of ground-layer aberration. The optical design of the GMT, with its Gregorian configuration and very fast primary mirror, conjugates the secondary to a plane 150 m above the ground, ideally suited for wide-field correction of the boundary layer.

ACKNOWLEDGEMENTS

This study has been supported by the National Science Foundation under award AST-0138347.

REFERENCES

1. R. Angel, J. Burge, J. L. Codona, W. Davison, and B. Martin, 2003, “20 and 30 m telescope designs with potential for subsequent incorporation into a track-mounted pair (20/20 or 30/30),” in *Future Giant Telescopes*, J. R. P. Angel and R. Gilmozzi, eds., Proc. SPIE **4840**, 183–193
2. J. R. P. Angel, M. Lloyd-Hart, E. K. Hege, R. J. Sarlot, and C. Peng, 2001, “The 20/20 telescope: MCAO imaging at the individual and combined foci,” in *Beyond Conventional Adaptive Optics*, R. Ragazzoni, ed. , **58**, 17–26

3. R. Angel and M. Lloyd-Hart, 2000, "Atmospheric tomography with Rayleigh laser beacons for correction of wide fields and 30 m class telescopes," in *Adaptive Optical Systems Technology*, P. L. Wizinowich, ed., Proc. SPIE **4007**, 270–276
4. M. Lloyd-Hart, J. Georges, R. Angel, G. Brusa, and P. Young, 2001, "Dynamically refocused Rayleigh laser beacons for atmospheric tomography," *Adaptive Optics Systems and Technology II*, R. K. Tyson, D. Bonaccini, and M. Roggemann, eds., Proc. SPIE **4494**, 259
5. J. A. Georges, P. Mallik, T. Stalcup, J. R. P. Angel, and R. Sarlot, 2003, "Design and testing of a dynamic refocus system for Rayleigh laser beacons," in *Adaptive Optical System Technologies II*, P. L. Wizinowich and D. Bonaccini, eds., Proc. SPIE **4839**, 473–483
6. J. A. Georges, T. Stalcup, and R. Angel, 2003, "Field tests of dynamic refocus of Rayleigh laser beacons," these proceedings
7. M. Lloyd-Hart and N. M. Milton, "Fundamental limits on isoplanatic correction with multi-conjugate adaptive optics," *JOSA A*, in press
8. R. Flicker, F. J. Rigaut, and B. L. Ellerbroek, 2000, "Comparison of multiconjugate adaptive optics configurations and control algorithms for the Gemini-South 8-m telescope," in *Adaptive Optical Systems Technology*, P. L. Wizinowich, ed., Proc. SPIE **4007**, 1032–1043
9. G. Rousset, "Wave-front sensors," in *Adaptive Optics in Astronomy*, ed. F. Roddier, (Oxford University Press, New York, 1999), 118
10. R. J. Noll, 1976, "Zernike polynomials and atmospheric turbulence," *J. Opt. Soc. Am.*, **66**, 207–211
11. D. L. McKenna, R. Avila, J. M. Hill, S. Hippler, P. Salinari, P. C. Stanton, and R. Weiss, 2003, "The LBT Facility SCIDAR: Recent Results," in *Adaptive Optical System Technologies II*, P. L. Wizinowich and D. Bonaccini, eds., Proc. SPIE **4839**, 825–836
12. F. Roddier, "Theoretical aspects," in *Adaptive Optics in Astronomy*, ed. F. Roddier, (Oxford University Press, New York, 1999), 36–37
13. B. L. Ellerbroek, F. Rigaut, B. Bauman, C. Boyer, S. Browne, R. Buchroeder, J. Catone, P. Clark, C. d'Orgeville, D. Gavel, G. Herriot, M. R. Hunten, E. James, E. Kibblewhite, I. McKinnie, J. Murray, D. Rabaut, L. Saddlemyer, J. Sebag, J. Stillburn, J. Telle, and J. Veran, 2003, "MCAO for Gemini-South," in *Adaptive Optical System Technologies II*, P. L. Wizinowich and D. Bonaccini, eds., Proc. SPIE **4839**, 55–66
14. J. N. Bahcall and R. M. Soneira, 1981, "Predicted star counts in selected fields and photometric bands: Applications to galactic structure, the disk luminosity function, and the detection of a massive halo," *Astrophysical Journal Supplement Series*, **47**, 357–401
15. F. Roddier, M. J. Northcott, J. E. Graves, and D. L. McKenna, 1993, "One-dimensional spectra of turbulence-induced Zernike aberrations: time-delay and isoplanicity error in partial adaptive compensation," *J. Opt. Soc. Am.*, **10**, 957–965
16. J. W. Hardy, *Adaptive Optics for Astronomical Telescopes*, (Oxford University Press, New York, 1998), 147–150
17. A. T. Tokunaga, "Infrared Astronomy," in *Allen's Astrophysical Quantities*, 4th Edition, ed. A. N. Cox, (AIP Press, Springer-Verlag, New York, 2000), 146